Far-Infrared Reflectivity of Sintered $YBa_2Cu_3O_7$ in the Normal and Superconducting State

W. Ose, P.E. Obermayer, H.H. Otto, T. Zetterer, H. Lengfellner, J. Keller, and K.F. Renk

Fakultät für Physik, Universität Regensburg, Federal Republic of Germany

We report on a study of the far-infrared reflection for a sintered $YBa_2Cu_3O_7$ sample that contained a large portion of preferentially oriented crystallites with the $a-b$ plane parallel to the surface and that showed extraordinary high far-infrared reflectivity. From experimental reflection data we determined, by Kramers-Kronig analysis, the dynamical conductivity and extracted the contributions due to free charge carriers and phonons, respectively. We find evidence for an anomalous behavior of the dynamical conductivity at temperatures above T_c; the dynamical conductivity increases strongly for temperatures approaching T_c and is strongly frequency dependent. By use of the Mattis-Bardeen theory we obtain an estimate for the superconducting energy gap of $2\Delta/kT_c \simeq 4.6$ (for $T \ll T_c$). We find that the lowest frequency infrared-active phonon mode is less damped in the superconducting state than in the normal state.

I. Introduction

Soon after the discovery of high-T_c superconductivity [1–3] far-infrared properties have been studied in order to determine superconducting energy gaps. For sintered $La-Sr-Cu-O$ compounds energy gaps (for $T \ll T_c$) of $2\Delta/kT_c \simeq 3.5$ [4–11] and for sintered $YBa_2Cu_3O_7$ values between 2.3 and 3.5 have been reported [12–22]. From a recent reflectivity study of single crystal platelets on a copper surface Schlesinger et al. [23] concluded an energy gap $2\Delta/kT_c \simeq 8$ for radiation with the electric field vector in the $a-b$ plane of the crystals.

In this paper we report far-infrared reflection measurements for a sintered $YBa_2Cu_3O_7$ sample that contained a large amount of preferentially oriented crystallites with the $a-b$ plane almost parallel to the sample surface and that showed extraordinary high far-infrared reflectivity. We will present an analysis of the reflectivity data that leads us to an estimate for the superconducting energy gap of $2\Delta/kT_c \simeq 4.6$. The analysis delivers, in addition, evidence for anomalous behavior of the dynamical conductivity at temperatures above T_c and for an influence of the superconducting state on the infrared-active phonons.

II. Sample Preparation and Characterization

For preparation of a sample appropriate amounts of highly pure Y_2O_3, $BaCO_3$ and CuO fine powders were mixed and pressed to a pellet at a pressure of 10 tons per cm^2. For elimination of residual contamination with H_2O and OH^- the pellet was heated for 10 h at about 500 °C in air, then sintered at 870 °C for 10 h and slowly cooled down to room temperature. Then the pellet was reground and the powder heated at 750 °C in flowing oxygen for 12 h. After cooling a new pellet was formed under the same pressure as before, sintered at 950 °C for 15 h in flowing oxygen and slowly cooled down over a period of 6 h, with an intermediate annealing stage at 550 °C for 2 h causing an optimal oxygen content of the superconducting phase. In our study the sample surface was untreated.

We studied the sample surface by electron scanning microscopy. Two typical pictures of different magnification are shown in Fig. 1. We found that the surface contained a large portion of crystallite plates (of typical area 2 μm · 8 μm); the orientation of neighbouring crystallites changes by 45° or 90°, i.e. the surface is in a relatively highly ordered state with regions of parquet-like texture.
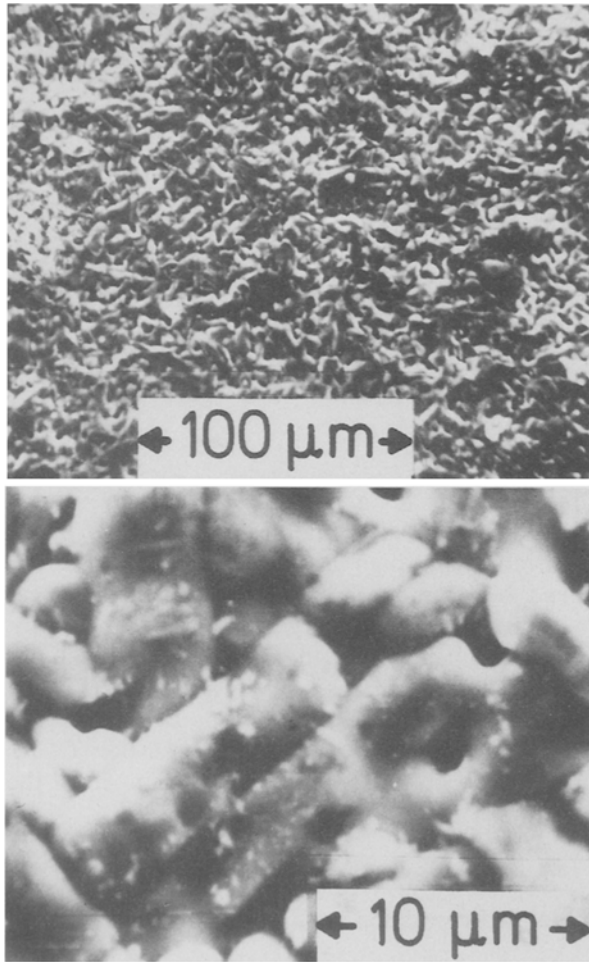
Fig. 1. Sample surface studied by electron scanning microscopy

For further characterization we performed X-ray diffraction experiments. A powder analysis by the Guinier method (Fig. 2a) shows that the material has orthorhombic structure. We obtained, for a temperature of 26 °C, the lattice parameters $a = 3.8194(8)$ Å, $b = 3.8883(8)$ Å, and $c = 11.668(2)$ Å. From these values an X-ray density of 6.39 g/cm³ follows; the average material density is 87% of the X-ray density. We have also performed an analysis by the Bragg-Brentano method with the disk plane of the pellet as a specimen surface and found (Fig. 2b) that the X-ray intensity of the 001 reflections is enhanced by more than 8 times compared to the Guinier diagram, indicating a remarkable texture of the crystallites in a surface range (of about 10 μm thickness) probed by the X-rays. Our results suggest that a large portion of the material was oriented with the $a - b$ plane almost parallel to the sample surface; pellets with preferentially oriented crystallites were used recently to study the anisotropy of the upper critical field [24]. The reason for the preferred orientation in the disk

plane after final pressing and subsequent sintering is the platy development of the crystallites, grown before the last sintering process, with the {001} pinacoid as habit determining form. Whereas the sample surface of the bulk shows a single phase X-ray diagram, we notice on the Guinier powder diagram some weak and relatively diffuse additional peaks, eventually resulting from a small amount of a secondary phase. Two of these peaks are indicated by question marks (Fig. 2a). The interplanar spacings of 5.453 Å and 3.148 Å suggest a Cu – Cu distance of 3.856 Å in the secondary phase. This value equals about $\frac{1}{2}(a + b)$ of the orthorhombic phase. We suggest that this phase occurs at the {110} twin boundaries.

The specific d.c. resistance (Fig. 3) was about $3 \mu\Omega m$ at room temperature and a third of this value at 110 K. The transition to superconductivity was sharp $(T_c \simeq 86 \text{ K})$. In a magnetic field the sample showed in comparison with a variety of other samples high levitation indicating a large Meißner effect. Using the relation between oxygen content and lattice parameters reported by Cava et al. [25] we found that the sample had the composition $YBa_2Cu_3O_{7+\delta}$ where $\delta = 0.1 \pm 0.1$. A large oxygen concentration, with $\delta > 0$, may be responsible for a value of T_c ($\simeq 86$ K) smaller than values ($\simeq 94$ K) known for samples with $\delta < 0$. (For samples prepared by a slightly different procedure we could also obtain large values of T_c, with zero resistance at 94 K; however, these samples showed smaller Meißner effect.)

III. Experimental Procedure

The reflection experiments were performed with a Fourier transform infrared spectrometer. The sample was mounted on a cold finger in a vacuum chamber of a temperature-variable cryostat. As optical window materials we used polyethylene at small frequencies ($\nu \leq 600$ cm⁻¹) and KBr at large frequencies. For radiation detection a liquid helium cooled bolometer was used at small frequencies and a liquid nitrogen cooled NiCdTe detector at large frequencies.

To obtain a reference, the superconducting sample was replaced by a gold mirror which consisted of a gold film (thickness > 1000 Å) evaporated on a glass plate. We have performed several different measurements in order to minimize errors by mechanical misalignment and suggest, from repeated experiments, an error of less than about 2% for our absolute reflectivity values that will be shown in the next chapter. The reflection measurements have been performed at small angles of incidence. The radiation was focused to a spot of 5 mm diameter; the angle of aperature was few degrees.
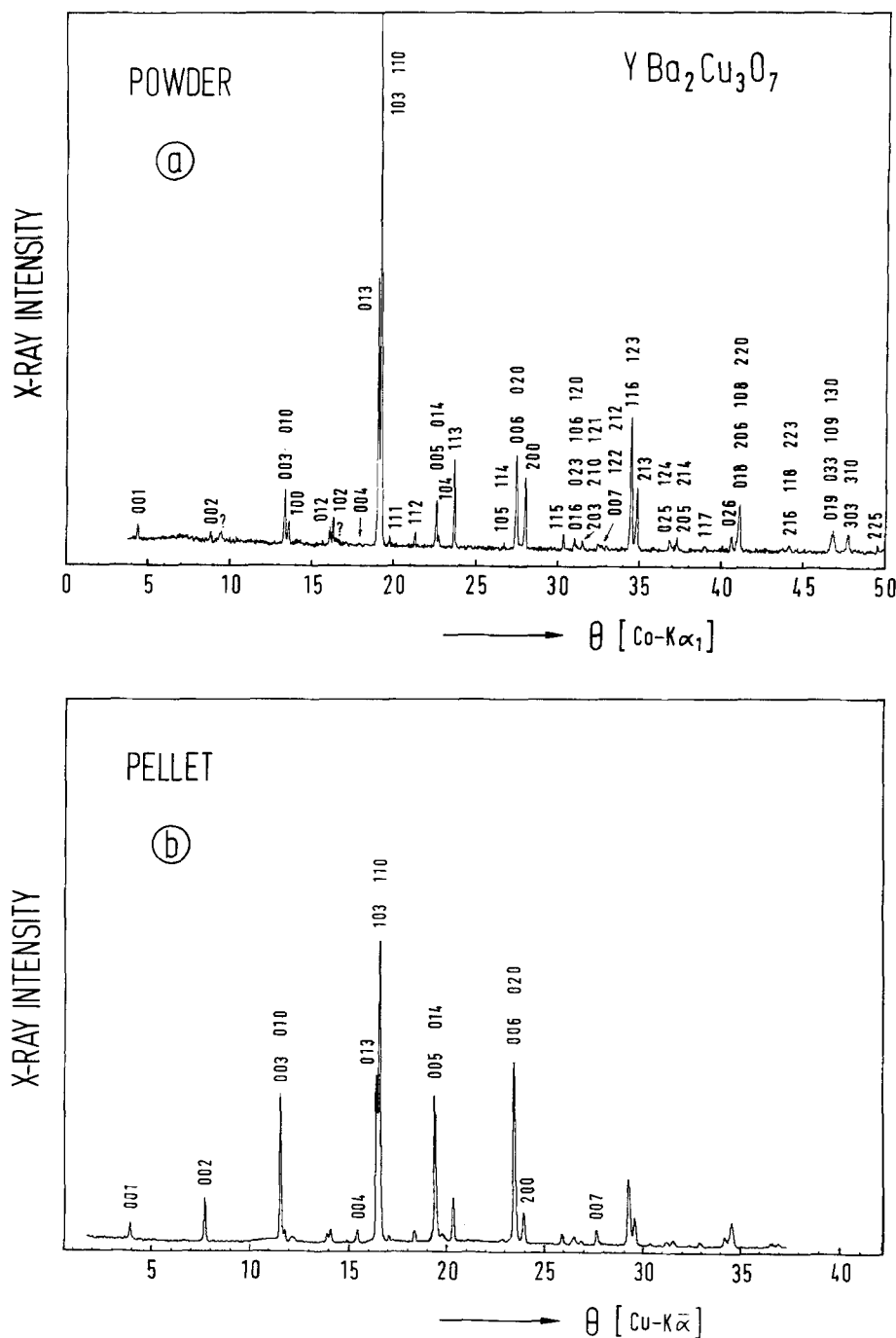
Fig. 2a and b. X-ray diffraction pattern of the sample used in the present experiment; (a), Guinier diagram of powder material using Co$-K_{\alpha_1}$ radiation ($\lambda = 1.78896$ Å) and (b), Bragg-Brentano diagram for the as-grown pellet with the disk plane as specimen surface using Cu$-K_{\bar{\alpha}}$ radiation ($\lambda = 1.54179$ Å)

We have also studied diffuse reflection, that is due to the roughness of the sample surface. Then we have chosen, for the sample at room temperature, a different arrangement. Radiation within a large solid angle (of almost π) was focused on the sample under oblique incidence (at an angle of incidence of about $\pi/4$). Radiation at an angle of reflection of $\pi/4$ (within a solid angle π) was collected and focused on the detector. By this technique a large part of diffusely reflected radiation in addition to the specularly reflected radia-

tion was collected. In other studies it was taken account of diffuse reflection by using the sample covered with a gold film as reference mirror. We did not use this technique in order to preserve our sample and especially the sample surface.

For the measurements an instrumental resolution of 1 cm^{-1} was chosen. However, to eliminate variations in the reflectivity curves that were clearly not related to the sample (such as interference in the cryostat windows and absorption lines of polyethylene)
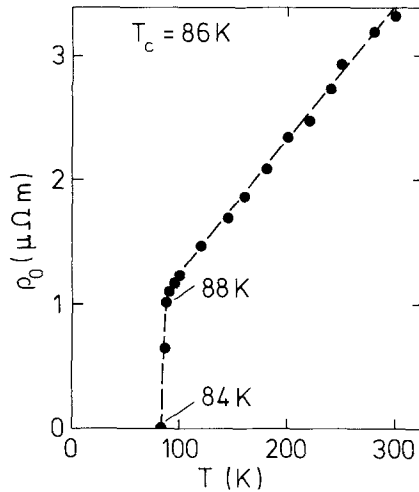
Fig. 3. Specific d.c. resistance ρ_0

Fig. 4. Far-infrared reflectivity of a YBa$_2$Cu$_3$O$_7$ sample for the normal state; inset, diffuse reflection behavior

Fig. 5. Far-infrared reflectivity for YBa$_2$Cu$_3$O$_7$ in the normal and superconducting state

we have averaged our reflectivity curves in limited frequency ranges. The effective resolution was therefore about 1 cm^{-1} in regions were structure related to the sample was clearly seen but about 10 cm^{-1} outside these regions.

IV. Experimental Results

Experimental reflection spectra for different temperatures above T_c are shown in Fig. 4. The reflectivity at room temperature (lower curve) is high at small frequencies and decreases towards larger frequencies. Cooling of the sample leads to a rather large increase of the reflectivity in the range of small frequencies. At large frequencies ($v > 600$ cm^{-1}) the reflectivity increases slightly if the temperature is lowered and remains almost independent of temperature for low temperatures, $T \leq 190$ K. The step-like structure in the reflectivity curves is due to infrared-active phonon modes. The reflectivity of our sample was almost specular at small frequencies (up to 600 cm^{-1}) and mainly diffuse at large frequencies (inset of Fig. 4); from the onset of diffuse reflection an average surface roughness of the order of few μm is estimated, which is in accordance with the electron microscope picture.

Figure 5 (dashed curve) shows a reflection spectrum for $T \ll T_c$. The reflectivity at small frequencies is almost constant and has a value of about 1. The original reflectivity data for the sample were slightly (by 2%) higher than for the gold mirror; since the gold mirror had an estimated reflectivity of 0.99 and since the reflectivity of the sample was almost independent of frequency, it is justified to assume a reflectivity of about 1 for the sample. The range of constant reflectivity extends to a very large frequency
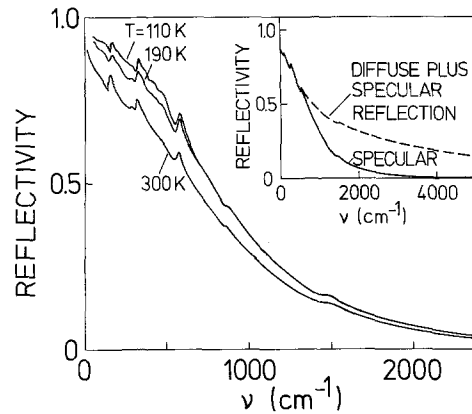
(130 cm^{-1}); this frequency corresponds to a minimal superconducting energy gap $2\Delta/kT_c \simeq 2.2$. The reflectivity for the superconducting state is enhanced, compared to the normal state, up to 380 cm^{-1} and is diminished at larger frequencies (Fig. 5). Below 380 cm^{-1} there is a strong increase of the reflectivity towards smaller frequencies. If we extrapolate the reflectivity curve with the experimental slope towards smaller frequencies we obtain a crossing point with the line of 100% reflectivity at 285 cm^{-1}. This value may be attributed to the superconducting energy gap; it corresponds to $2\Delta/kT_c \simeq 4.6$. A detailed analysis will be given in Chap. V.D. At low sample temperature (10 K) the specular reflectivity for large frequencies ($v > 600$ cm^{-1}) was almost the same as at 190 K.

The reflection spectrum for 10 K (Fig. 5) shows again pronounced phonon structure. However, instead of the step-like structure found for high temperatures, some of the phonons appear now as reflection minima; this is most evident for the lowest-frequency

resonance at 153 cm^{-1}. Clearly seen at all temparatures are four strong phonon resonances (one at 153 cm^{-1}, two near 300 cm^{-1}, and another at 570 cm^{-1}) and a weak resonance (at 192 cm^{-1}). Other structure (occurring mainly at low temperatures) is partly due to nonperfect elimination of absorption lines of the cryostat window material [26] and partly due to sample surface contamination with CO_2 rest gas in the cryostat; we found that already a small amount of CO_2 caused a broad absorption band near 200 cm^{-1}. The phonon structure will be discussed in Chap. V.E.

We have also performed reflection measurements on other samples. Though these were prepared in almost the same way as the sample of high far-infrared reflectivity, they showed much smaller reflectivities (with room temperature values between 10% and 40% as compared to 58% at 600 cm^{-1}). The main reason for the difference was a larger surface roughness, most likely resulting from a slightly higher sintering temperature than for the sample of high reflectivity.

For earlier studies of sintered $Y-Ba-Cu-O$ samples (and also for $La-Ba-Cu-O$) much smaller far-infrared reflectivities have been reported. The highest reflectivity values have been found by Thomas et al. [12], namely a reflectivity near 1 up to about 60 cm^{-1} but a decrease at larger frequencies. Our reflectivity curve for low temperature shows therefore that our sample and especially the surface range (with a thickness of typically 1000 Å that is probed by far-infrared radiation were of high quality. We note that Genzel [26] found, also for a sintered $YBa_2Cu_3O_7$ sample, similar high far-infrared reflectivities as our sample shows. In a single crystal study [23] a maximum increase of the reflectivity in the superconducting state compared to the normal state was found for a frequency of 500 cm^{-1}; this frequency was attributed to the superconducting energy gap $(2\Delta/kT_c \simeq 8)$.

V. Analysis

V.A. Concept of the Analysis

The sintered $YBa_2Cu_3O_7$ samples are spatially inhomogeneous (Fig. 1); there are regions of different orientations of crystallites, grain boundaries and holes in the material. For a description of the dynamical properties we introduce an effective complex dynamical conductivity $\sigma = \sigma_1 + i\sigma_2$.

In a first step we will perform a Kramers-Kronig analysis of the reflection data in order to determine the complex conductivity. In a further discussion we will determine the contributions to the conductivity by infrared-active phonons, free charge carriers and bound charge carriers, respectively. We therefore write the conductivity as a sum

$$\sigma = \sigma^p + \sigma^c + \sigma^b \qquad (1)$$

where $\sigma^p = \sigma_1^p + i\sigma_2^p$ is the contribution to the complex conductivity by phonons, $\sigma^c = \sigma_1^c + i\sigma_2^c$ by free charge carriers and $\sigma^b = \sigma_1^b + \sigma_2^b$ by bound charge carriers.

V.B. Kramers-Kronig Analysis and Conductivity at Room Temperature

Using the relationship

$$\Theta(v) = \frac{v}{\pi} \int_0^\infty \ln[R(v')](v^2 - v'^2)^{-1} \, dv' \qquad (2)$$

where v is the frequency (in cm^{-1}), Θ the phase shift of the reflected beam, we obtain the real part, n, and imaginary part, k, of the refractive index according to the relations $n = (1-R) N^{-1}$ and $k = 2R^{1/2} \sin\Theta \, N^{-1}$ where $N = (1-R^{1/2})^2 + 4R^{1/2} \sin^2(\Theta/2)$. It follows for the real part of the conductivity $\sigma_1 = 4\pi v c \varepsilon_0 nk$ and for the imaginary part $\sigma_2 = 2\pi v c \varepsilon_0 (n^2 - k^2)$ where c is the velocity of light in vacuum and $\varepsilon_0 = 8.9 \cdot 10^{-12}$ AsV^{-1} m^{-1}.

We will first discuss our procedure for the analysis of the room temperature reflectivity. In order to determine the conductivity in the range of our main interest (30 cm^{-1} to 600 cm^{-1}), we have also to know the reflectivities outside this range. For larger frequencies (600 cm^{-1} to 5000 cm^{-1}) we used the experimental curve that corresponds to the sum of specular and diffuse reflectivity (dashed in the inset of Fig. 4). For still larger frequencies we assumed a further decrease of the reflectivity and used the function $R(v) \simeq b_1 \exp(b_2/v)$ that allowed to solve the integral (2) analytically for large frequencies. We have chosen $b_1 = 0.05$ and $b_2 = 6 \cdot 10^3$ cm^{-1}. The function coincides with our experimental values near 5000 cm^{-1} and describes, approximately, reflection data at higher frequencies known for sintered samples [27, 28]. The extrapolated reflectivity values are, however, by a factor of two smaller than reported for the single crystal sample [23] and for crystalline thin films [29].

In the region of small frequencies ($v < 30$ cm^{-1}) we extrapolated our experimental curves by use of the Drude theory, with the Hagen-Rubens expression $1 - R = (8\varepsilon_0 vc/\bar{\sigma}_n)^{1/2}$ where $\bar{\sigma}_n$ is chosen in such a way that the experimental reflectivity curve is smoothly continued towards small frequencies.

For a survey we show in Fig. 6 the dynamical conductivities at room temperature for a large fre-
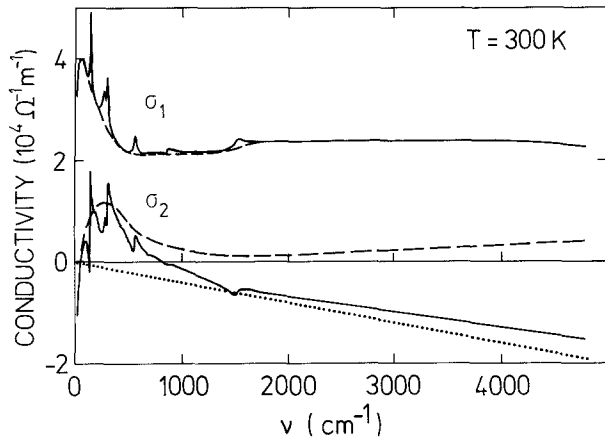
Fig. 6. Dynamical conductivities at room temperature obtained from Kramers-Kronig analysis (solid lines) and contribution by free charge carriers (dashed) and bound charge carriers (dotted)

quency range as obtained from the Kramers-Kronig analysis. The real part of the conductivity, σ_1, is almost constant at high frequencies and has a value $\sigma_n \simeq 2.3 \cdot 10^4 \; \Omega^{-1} \; \mathrm{m}^{-1}$. The corresponding dynamical resistance, $\rho_n \simeq 43 \; \mu\Omega\mathrm{m}$, is more than an order of magnitude larger than the d.c. resistance (Fig. 3). The reason for this discrepancy is not known; a similar discrepancy between dynamical and d.c. resistance has also been reported earlier [19]. The imaginary part, σ_2, of the dynamical conductivity (Fig. 6) is positive at small frequencies (ignoring the region of very small frequencies where the negative values arise from apparative limitations). It is negative at large frequencies and decreases almost linearly with frequency; the negative sign indicates that the imaginary part of the conductivity due to bound carriers is larger than for free carriers. Both the real part and the imaginary part of the conductivity (Fig. 6) show the phonon structure.

For an analysis of the smooth part of the conductivities, i.e. neglecting the phonon structure, we describe the contribution by free charge carriers at room temperature by a Drude term $\sigma^c = \sigma_n (1 - iv/v_\tau)^{-1}$ where v_τ is the scattering frequency for the free carriers and the contribution by bound charges by the expression $\sigma^b = -i(2\pi v c \varepsilon_0 \varepsilon_\infty)$ where ε_∞ is the high-frequency dielectric constant. Assuming a plasma frequency $v_p \simeq 17000 \; \mathrm{cm}^{-1}$, i.e. a free charge carrier concentration of about $5 \cdot 10^{21} \; \mathrm{cm}^{-3}$ at an effective mass equal to the free-electron mass, we find from $\sigma_n = 2\pi c \varepsilon_0 v_p^2/v_\tau$ a value $v_\tau \simeq 14000 \; \mathrm{cm}^{-1}$ and $v_p/v_\tau \simeq 1$. Similar values have already been reported for sintered material; for the single crystal sample [23] $v_p = 25000 \; \mathrm{cm}^{-1}$ and $v_\tau = 7000 \; \mathrm{cm}^{-1}$ have been used as parameters for description of the reflectivity. It follows that the imaginary part of the conductivity at high frequencies is

determined by both, the positive Drude term σ_2^c (dashed in Fig. 6) and the negative term σ_2^b (dotted). We find by this analysis a value $\varepsilon_\infty \simeq 2.4$. This value is smaller than most values discussed in earlier studies.

At small frequencies, the conductivities due to charge carriers (dashed curves in Fig. 6) do not show Drude behavior, that is characterized by $\sigma_1^c = \sigma_n$ and $\sigma_2^c \to 0$ for $v \to 0$, but show an enhancement. This additional conductivity will be discussed in the next chapter.

V.C. Evidence for Anomalous Conductivity at Temperatures above T_c

We find by the Kramers-Kronig analysis that the real part of the conductivity reaches for $v \geq 2000 \; \mathrm{cm}^{-1}$ constant values, namely for 300 K we have $\sigma_n \simeq 2.2 \cdot 10^4 \; \Omega^{-1} \; \mathrm{m}^{-1}$ and for low temperatures $\sigma_n \simeq 3.0 \cdot 10^4 \; \Omega^{-1} \; \mathrm{m}^{-1}$. The imaginary part at large frequencies is also slightly larger than at room temperature. The dynamical conductivities, obtained from the Kramers-Kronig analysis for different temperatures and for the range of smaller frequencies are shown in Fig. 7. We find a strong deviation from a normal Drude behavior; at small frequencies, there appears an anomalous conductivity with large values for both the real and the imaginary parts. When the temperature decreases and approaches T_c this anomalous conductivity increases. The real part, σ_1^c, increases towards smaller frequencies while the imaginary part, σ_2^c, shows a maximum. This behavior is clearly seen for $T = 110$ K (Fig. 7) and also for 300 K (Figs. 7 and 6); the experimental curve for 190 K shows a deviation from this behavior which is due to an experimental error in the reflection curve.

In Fig. 8 we have plotted, for $T = 110$ K, the real part of the *additional* conductivity, $\sigma_1^c - \sigma_n$, and also the imaginary part σ_2^c. The real part is large at small frequencies and decreases at larger frequencies. The imaginary part increases at small frequencies, has a maximum and then decreases. The additional conductivity can be fitted by a Drude formula $\sigma^a = \sigma_0^a(1 - iv/v_\tau^a)$ where $\sigma_0^a (\simeq 17 \cdot 10^4 \; \Omega^{-1} \; \mathrm{m}^{-1})$ is the conductivity for $v \to 0$ and $v_\tau^a(\simeq 70 \; \mathrm{cm}^{-1})$ a characteristic frequency. A negative sign of the additional conductivity in a part of the frequency scale (Fig. 8) is consistent with the sum rule for the real part of the conductivity. The conductivity at small frequencies (inset of Fig. 8) is strongly temperature dependent; the additional conductivity $\sigma_1^c - \sigma_n$ which is almost equal to σ_0^a varies approximately as $(T - T_c)^{-1}$ for $T > T_c$ (solid line). A comparison with the conductivities at different temperatures (Figs. 7 and 6) indicates that v_τ^a is strongly
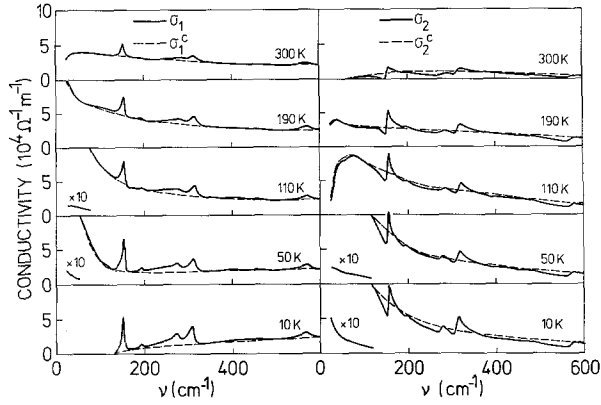
Fig. 7. Dynamical conductivities at different temperatures obtained from Kramers-Kronig analysis (solid lines) and contribution by free charge carriers (dashed)
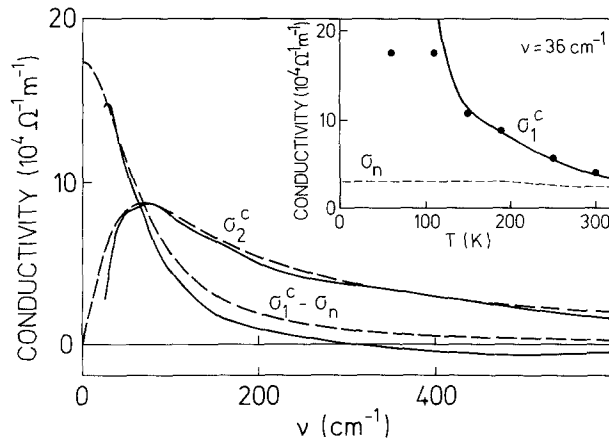

Fig. 8. Additional dynamical conductivities at 110 K according to experiment (solid lines) and theoretical description (dashed); inset, experimental conductivity σ_1^c at fixed frequency (points) and theoretical curve (solid), and conductivity for large frequencies, σ_n

temperature dependent; for $T=300$ K we find $v_\tau^a \simeq 250$ cm^{-1}.

The temperature dependence of the additional conductivity suggests an explanation by two-dimensional superconducting fluctuation, i.e. Cooper pairs formed by thermal fluctuations above T_c. For a first estimate we apply the theory of Aslamasov and Larkin [30] for the d.c. conductivity of thin films. Accordingly the additional d.c. conductivity due to fluctuations is

$$\Delta\sigma = e^2(16\hbar d\varepsilon)^{-1} \qquad (3)$$

where d is the film thickness and $\varepsilon = (T - T_c)/T_c$. As can be seen from the inset of Fig. 8 the experimental results for $\sigma_1^c - \sigma_n$ can be fitted quite well by (3) with $d \simeq 3 \times 10^{-10}$ m; a deviation at $T \sim T_c$ may be due to the fact that the experimental points are given for

a small but finite frequency. The value of d is of the order of the lattice spacing. Fluctuations of two-dimensional character therefore may be related to superconducting currents in the $a-b$ planes. We note that recent results of a d.c. conductivity measurement [31] on sintered YBa$_2$Cu$_3$O$_7$ have been interpreted by three-dimensional fluctuations. The frequency dependence of the conductivity due to fluctuation effects has been studied earlier for thin films both theoretically [32] and experimentally using far-infrared spectroscopy [33]. For temperatures $T > T_c$ (not too close to T_c) and not too small frequencies the frequency dependence of the conductivity due to fluctuations can be well approximated by a Drude formula with a characteristic frequency (in cm^{-1}) $v_\tau^a = 16 k_B T\varepsilon(hc)^{-1}$. The observed frequency dependence of the dynamical conductivity is therefore also consistent with superconducting fluctuations.

In an alternative explanation the additional conductivity may be attributed to free charge carriers in a second band with a strongly temperature dependent scattering rate which becomes small at low temperatures; the maximum of σ_0^a at $T \sim T_c$ would then be a consequence of the superconducting transition. Such free charge carriers may be due to quasiparticle states arising from interaction and nesting effects on the Fermi surface of the two-dimensional electron system [34]. With the relation $\sigma_0^a = 2\pi c v_{p,a}^2/v_\tau^a$ we obtain a plasma frequency $v_{p,a}$ for the second charge carriers type. We find $v_{p,a} \simeq 2700$ cm^{-1} for $T \simeq 110$ K, i.e. the corresponding concentration may be much smaller than for the normal charge carries (or the concentration may be similar but the effective mass much larger). It follows in this interpretation that the excitations in the second band are only weakly damped at 110 K ($v_{p,a}/v_\tau^a \simeq 40$); for 300 K (Fig. 6) $v_{p,a}$ and therefore the carrier concentration are comparable to the values at 110 K while the scattering rate is strongly increased.

V.D. Superconducting Properties

In Fig. 9 we have drawn the real and imaginary parts of the conductivity that we obtained by subtracting, according to (1), the contributions by phonons (Chap. V.E.) and bound charge carriers. The real part of the dynamical conductivity, σ_1^c, is zero up to 130 cm^{-1} and increases to σ_n at large frequencies. The imaginary part, σ_2^c, is large at small frequencies and decreases with increasing frequency. In the range of large frequencies (not shown in Fig. 9) σ_2^c shows Drude behavior, i.e. it increases linearly with frequency as at room temperature (dashed in Fig. 6). At smaller frequencies ($v \leq 600$ cm^{-1}) this linear por-
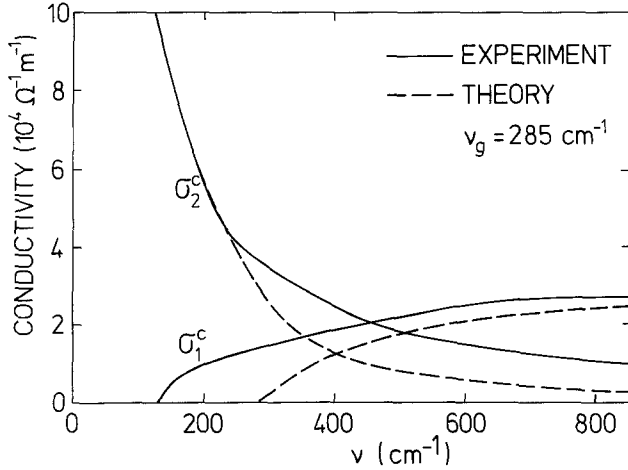
Fig. 9. Dynamical conductivities at low temperature ($T \simeq 10$ K) according to our experiment (solid line) and to the Mattis-Bardeen theory (dashed)

Fig. 10. Dynamical resistivities at low temperature ($T \simeq 10$ K); solid lines, experiment; dotted, Mattis-Bardeen theory with $v_g = 285$ cm^{-1} ($2\Delta/kT_c = 4.6$); dashed, theory with a rectangular distribution of gaps in the range $2.2 \leqq 2\Delta/kT_c \leqq 8$

tion to σ_2^c is small and therefore we subtracted it for simplicity from the experimental values and obtained for σ_2^c the solid curve of Fig. 9. For comparison we show the conductivity expected from the theory of Mattis and Bardeen [35, 36] (dashed) for superconductors in the dirty limit for $T \ll T_c$. The theory contains only one parameter, the gap frequency v_g. With a value $v_g = 285$ cm^{-1} we can well describe σ_2^c for small frequencies, while the calculated conductivity at large frequencies is smaller than the experimental values. The experimental cut-off frequency for σ_1^c is smaller than the assumed gap frequency. We suggest that the inhomogeneity of the sample may be a reason for the differences between theory and experiment. We have therefore performed a slightly modified analysis which will be discussed in the following.

According to the microscopic picture (Fig. 1) there are small conducting crystallites that have connections with each other. The corresponding grain boundary regions and also polysynthetic twin boundary regions may have resistivities different from those of ideal crystal regions. Since all structures are much smaller than the wavelengths of far-infrared radiation it might be reasonable to discuss a series of resistivities that determines the dynamical conductivity at far-infrared frequencies. We therefore introduce the complex dynamical resistivity $\rho_1 + i\rho_2 = (\sigma_1^c + i\sigma_2^c)^{-1}$ where ρ_1 is the resistance and ρ_2 the reactance. In Fig. 10 we show resistivity curves (solid line) obtained from the experimental values of σ_1^c and σ_2^c and theoretical curves (dotted) that follow from the Mattis-Bardeen theory for $v_g = 285$ cm^{-1}; this value is now chosen in such a way that the maxima for both the experimental and theoretical ρ_2 curves coincide. The theoretical resistance is zero for $v < v_g$ and increases
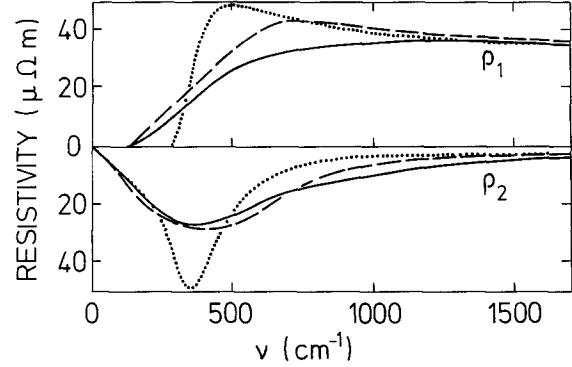
to a maximum value at $v \simeq 1.7 v_g$ and then decreases to $\rho_n = 1/\sigma_n$ at larger frequencies. The absolute value of the reactance has a maximum for $v \simeq 1.25 v_g$; for small frequencies ($v < v_g$) $\rho_2 = 1/\sigma_2^c$ and for large frequencies ($v > v_g$) ρ_2 is proportional to σ_2^c. In comparison with the theory the experimental curves are broadened. This behavior may be described by assuming that there exists a distribution of energy gaps. Assuming a rectangular distribution of energy gaps, in the range 130 cm^{-1} to 480 cm^{-1}, we find the dashed curves. Thus, the complex resistivity behaves as we would have a distribution of energy gaps in the range $2.2 \leqq 2\Delta/kT_c \leqq 8$. A distribution of different energy gaps may be attributed to grains of slightly different electronic structure and also to the anisotropy of the differently oriented crystallites. Anisotropic pairing states which have been proposed for heavy-fermion superconductors are also discussed for the high-temperature superconductors [37, 38]. The range of energy gaps suggested from our study is consistent with results of tunnel experiments [39].

V.E. Infrared-Active Phonons

We describe the dynamical conductivity due to photons by Lorentzian resonances

$$\sigma^p = -i(2\pi v c \varepsilon_0) \sum_j S_j v_j^2 (v_j^2 - v^2 - i\Gamma_j v)^{-1} \qquad (4)$$

where S_j, v_j, and Γ_j are oscillator strength, eigenfrequency and damping of the jth phonon mode, respectively. Table 1 shows parameters that follow from the conductivity curves (Fig. 7). The $j = 1$ resonance is most likely mainly due to vibrations of the Ba ions against oxygen ions, the $j = 2$ resonance to vibrations of Y against oxygen ions and the other modes to Cu $-$ O vibrations. The resonance frequencies (Ta-

Table 1. Eigenfrequencies, oscillator strengths and damping constants for infrared-active phonons

j	$v(\text{cm}^{-1})$		S_j		$\Gamma_j(\text{cm}^{-1})$	
	10 K	110 K	10 K	110 K	10 K	110 K
1	153		3	5	4	7
2	192		0.5	0.5	10	
3	276	278	1	0.8	15	
4	308	312	1.5	1.3	15	
5	565	567	0.23	0.19	20	

ble 1) extend up to about $600\ \text{cm}^{-1}$; Raman-active phonons are found in the same frequency range [15, 40–43]. We suggest that the structure in the conductivity curves at large frequencies (Fig. 6) is due to phonon combination absorption. The structure near $900\ \text{cm}^{-1}$ and $1550\ \text{cm}^{-1}$ (Fig. 6) may correspond to two and three phonon processes, respectively. High-frequency cut-off frequencies (near $1200\ \text{cm}^{-1}$ and $1800\ \text{cm}^{-1}$) are consistent with a maximum phonon frequency of $600\ \text{cm}^{-1}$ in the phonon density of states as obtained from a lattice dynamical study [41].

We find that the $j=3$, 4 and 5 phonons (Table 1) are slightly softer in the superconducting state; phonon softening effects for the $j=3$ and 4 infrared-active phonons and for Raman-active phonons are known from recent studies [15, 21, 40]. At high temperatures (above 190 K) the oscillator strengths of all phonon resonances decrease with increasing temperature (Fig. 7). The transition from the normal to the superconducting state influences the resonances differently (Table 1), namely the $j=2$ phonon is uninfluenced, the $j=3$, 4 and 5 phonons show a small increase of oscillator strength but no change of the halfwidth; i.e. these phonons have negligible or weak interaction with the charge carriers of the superconducting state. For the $j=1$ phonon both the oscillator strength and the halfwidth decrease by a factor of two (Table 1). This indicates that the $j=1$ phonon has a direct interaction with the charge carriers that are responsible for the superconductivity. Weaker damping may occur because the quantum energy of a phonon is not sufficient to break up a Cooper pair. Since the $j=1$ phonon (with strong $Ba-O$ amplitudes) is a vibration of ions near the $Cu-O$ $a-b$ planes the observed interaction of this vibration with Cooper pairs is consistent with superconductivity in these planes.

VI. Conclusion

In this paper we report results of a study of the far-infrared reflectivity and dynamical conductivity of $YBa_2Cu_3O_7$. We find evidence for anomalous behav-

ior of the dynamical conductivity above T_c that may either be due to superconducting fluctuations or by normal charge carriers with a small scattering rate. We determine for the superconducting energy gap for $T \ll T_c$ a value $2\Delta/kT_c \simeq 4.6$ that is larger than values concluded from earlier far-infrared studies on sintered high-T_c superconductors but smaller than a value of 8 concluded from a study of a crystalline sample. We observe an influence of the superconductivity on phonon modes; especially the lowest-frequency phonon is less damped in the superconducting state than in the normal state. Our results give support for two-dimensional character of the superconductivity.

Finally we want to remark that the reflectivity of our sample is extraordinarily high. Besides a good flatness, the preferred orientation of crystallites in the sample surface with their c-axes perpendicular to the surface and a good contact behavior for the dynamical currents between different crystallites may be important for the high reflectivity. The high quality of our sample made it possible to obtain new information about the superconducting state in $YBa_2Cu_3O_7$ which will be useful for further experimental and theoretical investigation.

References

1. Bednorz, J.G., Müller, K.A.: Z. Phys. B – Condensed Matter 64, 189 (1986);
Bednorz, J.G., Takashige, M., Müller, K.A.: Europhys. Lett. 3, 379 (1987)
2. Wu., M.K., Ashburn, J., Torng, C.J., Hor, P.H., Meng, R.L., Gao, L., Huang, Z.J., Wang, Y.Q., Chu, C.W.: Phys. Rev. Lett. 58, 908 (1987)
3. Zhao, Z., Chen, Z., Yang, Q., Huang, Y., Chen, C., Tang, R., Liu, G., Cui, C., Chen, L., Wang, L., Guo, S., Li, S., Bi, J.: Kexue Gongbao Chin. Ed. 32, 6 (1987)
4. Sulewski, P.E., Sievers, A.J., Buhrman, R.A., Tarascon, J.M., Greene, L.H.: Phys. Rev. B 35, 5330 (1987)
5. Schlesinger, Z., Greene, R.L., Bednorz, J.G., Müller, K.A.: Phys. Rev. B 35, 5334 (1987)
6. Walter, U., Sherwin, M.S., Stacy, A., Richards, P.L., Zettl, A.: Phys. Rev. B 35, 5327 (1987)
7. Sulewski, P.E., Sievers, A.J., Buhrman, R.A., Tarascon, J.M., Greene, L.H., Curtin, W.A.: Phys. Rev. B 35, 8829 (1987)
8. Bonn, D.A., Greedan, J.E., Stager, C.V., Timusk, T.: Solid State Commun. 62, 383 (1987)
9. Bonn, D.A., Greedan, J.E., Stager, C.V., Timusk, T., Doss, M.G., Herr, S.L., Kamaras, K., Porter, C.D., Tanner, D.B., Tarascon, J.M., McKinnon, W.R., Greene, L.H.: Phys. Rev. B 35, 8843 (1987)
10. Schlesinger, Z., Collins, R.T., Shafer, M.W., Engler, E.M.: Phys. Rev. B 36, 5275 (1987)

11. Sulewski, P.E., Noh, T.W., McWhirter, J.T., Sievers, A.J.: Phys. Rev. B **36**, 5735 (1987)
12. Thomas, G.A., Ng, H.K., Millis, A.J., Bhatt, R.N., Cava, R.J., Rietman, E.A., Johnson, Jr., D.W., Epinosa, G.P., Vanderberg, J.M.: Phys. Rev. B **36**, 846 (1987)
13. Bonn, D.A., Greedan, J.E., Stager, C.V., Timusk, T., Doss, M.G., Herr, S.L., Kamarás, K., Tanner, D.B.: Phys. Rev. Lett. **58**, 2249 (1987)
14. Genzel, L., Wittlin, Kuhl, A., Mattausch, Hj., Bauhofer, W., Simon, A.: Solid State Commun. **63** 843 (1987)
15. Cardona, M., Genzel, L., Liu, R., Wittlin, A., Mattausch, Hj., Garcia-Alvaredo, R., Garcia-Gonzales, E.: Solid State Commun.: (to be published)
16. Onari, S., Iioka, M., Ohshima, K., Arai, T., Sakudo, T.: Jpn. J. Appl. Phys. **26**, L1052 (1987)
17. Collins, R.T., Schlesinger, Z., Koch, R.H., Laibowitz, R.B., Plaskett, T.S., Freitas, P., Gallagher, W.J., Sandstrom, R.L., Dinger, T.R.: Phys. Rev. Lett. **59**, 704 (1987)
18. Wrobel, J.M., Wang, S., Gygax, S., Clayman, B.P., Peterson, L.K.: Phys. Rev. B **36**, 2368 (1987)
19. Sulewski, P., Noh, T.W., McWhirter, J.T., Sievers, A.J., Russek, S.E., Buhrman, R.A., Jee, C.S., Crow, J.E., Salomon, R.E., Meyer, G.: Phys. Rev. B **36**, 2357 (1987)
20. Noh, T.W., Sulewski, P.E., Sievers, A.J.: (to be published)
21. Wittlin, A., Liu, R., Cardona, M., Genzel, L., König, W., Bauhofer, W., Mattausch, Hj., Simon, A.: Solid State Commun. **64**, 477 (1987)
22. Renk, K.F., Lengfellner, H., Obermayer, P.E., Ose, W., Otto, H.H., Zetterer, T., Schindler, W., Saemann-Ischenko, G.: Intl. J. IR and MM Waves, December 1987
23. Schlesinger, Z., Collins, R.T., Kaiser, D.L., Holtzberg, F.: Phys. Rev. Lett. **59**, 1958 (1987)
24. Takita, K., Akinaga, H., Katoh, H., Uchino, T., Ishigaki, T., Asano, H.: Jpn. J. Appl. Phys. **26**, L1323 (1987)
25. Cava, R.J., Batlogg, B., Chen, C.H., Rietman, E.A., Zakurak, S.M., Werder, D.: Nature **329**, 423 (1987)
26. Genzel, L.: Private communication
27. Bozovic, I., Kirillov, D., Kapitulnik, A., Char, K., Hahn, M.R., Beasley, M.R., Geballe, T.H., Kim, Y.H., Heeger, A.J.: Phys. Rev. Lett. **59**, 2219 (1987)
28. Wang, X., Nanba, T., Ikezawa, M., Isikawa, Y., Mori, K., Kobayashi, K. Kasai, K., Sato, K., Fukase, T.: Jpn. J. Appl. Phys. **26**, L1391 (1987)
29. Orenstein, J., Thomas, G.A., Rapkine, D.H., Bethea, C.G., Levine, B.F., Cava, R.J., Rietman, E.A., Johnson, Jr., D.W.: Phys. Rev. B **36**, 729 (1987)
30. Aslamasov, L.G., Larkin, A.I.: Phys. Lett. **26**A, 238 (1968)
31. Freitas, P.P., Tsuei, C.C., Plaskett, T.S.: Phys. Rev. B **36**, 833 (1987)
32. Skocpol, W.J., Tinkham, M.: Rep. Progr. Phys. **38**, 1049 (1975)
33. Tanner, D.B.: Phys. Rev. B **8**, 5045 (1973)
34. Rice, T.M.: Z. Phys. B – Condensed Matter **67**, 141 (1987)
35. Mattis, D.C., Bardeen, J.: Phys. Rev. **111**, 412 (1958)
36. Tinkham, M.: In: Far infrared properties of solids. Mitra, S.S., Nudelman, S., (eds.). New York: Plenum Press 1970
37. Ohkawa, F.J.: Jpn. J. Appl. Phys. **26**, L652 (1987)
38. Maekawa, S., Ebisawa, H., Isawa, Y.: Jpn. J. Appl. Phys. **26**, L468 (1987)
39. Kirtley, J.R., Collins, R.T., Schlesinger, Z., Gallagher, W.J., Sandstrom, R.L., Dinger, T.R., Chance, D.A.: Phys. Rev. B **35**, 8846 (1987)
40. Macfarlane, R.M., Rosen, H., Seki, H.: Solid State Commun. **63**, 831 (1987)
41. Stavola, M., Krol, D.M., Weber, W., Sunshine, S.A., Jayaraman, A., Kourouklis, G.A., Cava, R.J., Rietman, E.A.: Phys. Rev. B **36**, 850 (1987)
42. Battlog, B., Cava, R.J., Jayaraman, A., van Dover, R.B., Kourouklis, G.A., Sunshine, S., Murphy, D.W., Rupp, L.W., Chen, H.S., White, A., Mujsce, A.M., Rietmann, E.A.: Phys. Rev. Lett. **58**, 2333 (1987)
43. Yamanaka, A., Miniami, F., Watanabe, K., Inoue, K., Takekawa, S., Iyi, N.: Jpn. J. Appl. Phys. **26**, L1404 (1987)

W. Ose, P.E. Obermayer, H.H. Otto, T. Zetterer,
H. Lengfellner, J. Keller, K.F. Renk
Fakultät für Physik
Universität Regensburg
Universitätsstrasse 31
D-8400 Regensburg
Federal Republic of Germany